Numerical simulation of photoexcited polaron states in water

E. V. Zemlyanaya, A. V. Volokhova, V. D. Lakhno, I. V. Amirkhanov, I. V. Puzynin, T. P. Puzynina, V. S. Rikhvitskiy, and P. Kh. Atanasova

Citation: AIP Conference Proceedings **1684**, 100006 (2015); doi: 10.1063/1.4934343
View online: http://dx.doi.org/10.1063/1.4934343
View Table of Contents: http://scitation.aip.org/content/aip/proceeding/aipcp/1684?ver=pdfcov
Published by the AIP Publishing

Numerical Simulation of Photoexcited Polaron States in Water

E.V.Zemlyanaya[1,a)], A.V.Volokhova[1], V.D.Lakhno[2], I.V.Amirkhanov[1], I.V.Puzynin[1], T.P.Puzynina[1], V.S.Rikhvitskiy[1] and P.Kh.Atanasova[3]

[1]*Laboratory of Information Technologies, Joint Institute for Nuclear Research, Dubna 141980, Russia*
[2]*Institute of Mathematical Problems of Biology, Russian Academy of Science, Pushchino 142290, Russia*
[3]*Faculty of Mathematics and Informatics, Paisii Hilendarski University of Plovdiv 4003, Bulgaria*

[a)]Corresponding author: elena@jinr.ru

Abstract. We consider the dynamic polaron model of the hydrated electron state on the basis of a system of three nonlinear partial differential equations with appropriate initial and boundary conditions. A parallel numerical algorithm for the numerical solution of this system has been developed. Its effectiveness has been tested on a few multi-processor systems. A numerical simulation of the polaron states formation in water under the action of the ultraviolet range laser irradiation has been performed. The numerical results are shown to be in a reasonable agreement with experimental data and theoretical predictions.

INTRODUCTION

Solvated (hydrated) electron states arise as a result of the radiolysis in condensed media [1]. Such states can be considered as the capture of an excess electron by a potential well formed as a result of the polarization of medium molecules by the electron. Intensive attention to theoretical and experimental investigations of solvated electrons is related to the fact that a number of chemical processes occurs with their participation in nonorganic and organic chemistry. Hydrated electrons, which are the strongest reducer in water, are of special interest. In biological systems, the hydrated electron plays important role in processes of long-distance charge transfer. The dynamics of the absorption spectra during hydrated-electron formation in irradiated water gives important information about its structure and the kinetics of chemical reactions with its participation. Modern femtosecond spectroscopic methods allow one to understand a mechanism of the formation of hydrated electrons excited in pure water by means of the laser irradiation.

In [2], the polaron model of hydrated electron was suggested. It is shown, that theoretical estimations of the laser radiation absorption dynamics in ultra-violet range are in qualitative agreement with experimental data from [3]. In [4, 5], the numerical method for solving the system of nonlinear partial differential equations describing the dynamical polaron model, has been developed. The results of numeral simulation of the hydrated electron formation process are in agreement with experimental data of absorption of light in the polarized water [6].

In this contribution, we describe a parallel numerical scheme on the basis of the partition method [7] for investigation of the dynamical polaron model. The methodical calculations with the different amount of parallel processors and knots of discrete grid on spatial coordinate have been performed to confirm an efficiency of the parallel algorithm. Results of numerical simulation are presented in comparison with experimental data and theoretical estimations.

MATHEMATICAL MODEL

The theoretical approach is developed in [2] on a basis of the translation-invariant Landau – Pekar theory [8]. The equations describing a time-dependence of the wave polaron function Ψ the polarization potential Φ, follow from the

Application of Mathematics in Technical and Natural Sciences
AIP Conf. Proc. 1684, 100006-1–100006-9; doi: 10.1063/1.4934343

total energy functional of optical Pekar's polaron. These equations are as follows [2]:

$$i\hbar\dot{\Psi}(\vec{r},\tau) = -\frac{\hbar^2}{2m_0}\,\Delta\Psi(\vec{r},\tau) - e\Phi(\vec{r},\tau)\Psi(\vec{r},\tau), \tag{1}$$

$$\frac{1}{4\pi\omega^2 c}\,\Delta\ddot{\Phi}(\vec{r},\tau) + \gamma\Delta\dot{\Phi}(\vec{r},\tau) + \frac{1}{4\pi c}\,\Delta\Phi(\vec{r},\tau) + e|\Psi(\vec{r},\tau)|^2 = 0. \tag{2}$$

Here, $\hbar$ is the Plank constant, m_0 – the effective electron mass, $c = \varepsilon_\infty^{-1} - \varepsilon_0^{-1}$, ε_∞ and ε_0 – the high-frequency and static constants, e – the elementary charge, ω – the frequency of optical polarization medium oscillations, $\gamma = \tilde{\epsilon}/(\omega^2\tau_0)$ is a relaxation coefficient, τ_0 – the dielectric relaxation time, $\tilde{\epsilon}$ – coefficient of dielectric permeability. We put

$$\Delta\Phi(\vec{r},t) = \theta(\vec{r},\tau), \tag{3}$$

where θ has a physical sense of a density of polarized charge induced by electron. Thus, the equation (2) can be transformed to the form:

$$\frac{1}{4\pi\omega^2 c}\,\ddot{\theta}(\vec{r},\tau) + \gamma\Delta\dot{\theta} + \frac{1}{4\pi c}\,\theta(\vec{r},\tau) + e|\Psi(\vec{r},\tau)|^2 = 0. \tag{4}$$

Equations (1),(3),(4) determine the dynamical polaron model in the three-dimensional case. Substituting the expansions of the functions $\Psi(\vec{r},\tau)$ and $\Phi(\vec{r},\tau)$, $\theta(\vec{r},\tau)$ in terms of the spherical harmonics $Y_{lm_s}(\theta_s,\varphi_s)$

$$\Psi(\vec{r},\tau) = \sum_{l=0}^{\infty}\sum_{m_s=-l}^{l}\frac{\psi_{lm_s}(r,\tau)}{r}Y_{lm_s}(\theta_s,\varphi_s),$$

$$\Phi(\vec{r},\tau) = \sum_{l=0}^{\infty}\sum_{m_s=-l}^{l}\frac{\varphi_{lm_s}(r,\tau)}{r}Y_{lm_s}(\theta_s,\varphi_s),$$

$$\theta(\vec{r},\tau) = \sum_{l=0}^{\infty}\sum_{m_s=-l}^{l}\frac{\Theta_{lm_s}(r,\tau)}{r}Y_{lm_s}(\theta_s,\varphi_s)$$

into (1),(3),(4) and restricting our consideration to the spherically symmetric case of m_s=l=0, we obtain the system of spatially one-dimensional partial differential equations with respect to radial components $\psi_{00}(r,\tau)$, $\varphi_{00}(r,\tau)$ and $\Theta_{00}(r,\tau)$ of functions Ψ, Φ and θ.

Then, from dimensional time τ and coordinate r we come to the dimensionless variables t and x by means of the relations $\tau = t\cdot t_0$ and $r = x\cdot r_0$, where $r_0 = r_{00}\cdot a$, $a = 0.529\cdot 10^{-8}$ cm is the Bohr radius, $r_{00} = \sqrt{t_{00}} = \sqrt{t_0/t_{A0}} = 164.64$ is the scaling factor, $t_0 = 1/\omega_0$, $\omega_0 = 1.5246\cdot 10^{12}$ s^{-1} is the frequency of the medium oscillations, and $t_{A0} = 2.42\cdot 10^{-17}$s is the atomic time unit. Scaling is introduced to equalize the initial values of the physical parameters which differ by ten orders or more. In this case, the integration interval over the spatial variable decreases significantly (in accordance with the law $x = r/r_{00}$), which simplifies computer simulation.

The relation between the effective mass m_0 of the hydrated electron, the frequency ω of optical polarization medium oscillations, the relaxation coefficient γ and the respective dimensionless parameters $\bar{m}$, $\bar{\omega}$, $\bar{\gamma}$ is determined by the expressions $m_0 = \bar{m}\cdot m_e$ (where m_e is the electron mass in vacuum), $\omega = \bar{\omega}/t_0$, and $\gamma = \bar{\gamma}/t_0$.

Final form of the system of equations is as follows (here and hereafter, the subscripts 00 of functions ψ_{00}, φ_{00} and Θ_{00} are omitted):

$$\begin{cases} \left[i2\bar{m}\dfrac{\partial}{\partial t} + \dfrac{\partial^2}{\partial x^2} + 2\bar{m}\dfrac{r_{00}}{\tilde{\epsilon}}\dfrac{\varphi(x,t)}{x}\right]\psi(x,t) = 0, \\ \dfrac{\partial^2}{\partial x^2}\varphi(x,t) = \Theta(x,t), \\ \left[\dfrac{\partial^2}{\partial t^2} + \bar{\gamma}\dfrac{\partial}{\partial t} + \bar{\omega}^2\right]\Theta(x,t) = -\bar{\omega}^2\dfrac{|\psi(x,t)|^2}{x}. \end{cases} \tag{5}$$

Boundary conditions are following:

$$\varphi(0,t) = \varphi'(\infty,t) = 0,\ \ \psi(0,t) = \psi(\infty,t) = 0,\ \ \Theta(0,t) = \Theta(\infty,t) = 0. \tag{6}$$

Equations (5) with boundary conditions (6) describe the evolution of the state given at the initial condition of time. Here, $\tilde{\epsilon} = 1.81$, $\bar{m} = 2.692$, $\bar{\gamma} = 2.145$, and $\bar{\omega} = 1$ are the dimensionless parameters of the model.

NUMERICAL APPROACH

Finite Difference Scheme

For numerical solution, the system of differential equations (5) is replaced with that of difference equations on a uniform discrete mesh with nodes $x_m = m \times h_x$ and $t_n = n \times h_t$, where h_x and h_t are, respectively, the spatial stepsize and the time stepsize. As a result of substitutions of well-known finite-difference formulas [9], we obtain a system of difference equations with respect of $\psi_m^n = \psi(x_m, t_n)$, $\phi_m^n = \phi(x_m, t_n)$, $\Theta_m^n = \Theta(x_m, t_n)$:

$$\frac{\psi_m^{n+1} - \psi_m^n}{h_t} = i\left\{\sigma\left[\frac{\psi_{m+1}^{n+1} - 2\psi_m^{n+1} + \psi_{m-1}^{n+1}}{2\bar{m}h_x^2} + \frac{r_{00}}{\tilde{\epsilon}}\frac{\varphi_m^{n+1}}{\bar{m}h_x}\psi_m^{n+1}\right] + (1-\sigma)\left[\frac{\psi_{m+1}^{n} - 2\psi_m^{n} + \psi_{m-1}^{n}}{2\bar{m}h_x^2} + \frac{r_{00}}{\tilde{\epsilon}}\frac{\varphi_m^{n}}{\bar{m}h_x}\psi_m^{n}\right]\right\},$$

$$\frac{\varphi_{m+1}^{n+1} - 2\varphi_m^{n+1} + \varphi_{m-1}^{n+1}}{h_x^2} = \Theta_m^{n+1}, \quad (m = 1, 2, \ldots, l; \quad n = 0, 1, 2, \ldots; \quad \sigma = 0.5), \tag{7}$$

$$\frac{\Theta_m^{n+1} - 2\Theta_m^n + \Theta_m^{n-1}}{h_t^2} + \bar{\gamma}\frac{\Theta_m^{n+1} - \Theta_m^n}{h_t} + \bar{\omega}^2\Theta_m^{n+1} = -\bar{\omega}^2\frac{\left|\psi_m^n\right|^2}{\bar{m}h_x},$$

$$\Theta_m^{-1} = -\frac{\left|\psi_m^0\right|^2}{\bar{m}h_x}; \quad \Theta_m^0 = \Theta_m^{-1}; \quad \varphi_0^n = 0; \quad \varphi_l^n = \varphi_{l-1}^n; \quad \psi_0^n = \psi_l^n = 0$$

To solve this system, we used the algorithm described in [4] making it possible to sequentially calculate $\Theta(x_m, t_n)$, $\varphi(x_m, t_n)$, and $\psi(x_m, t_n)$ at nodes of the discrete mesh along the x axis under given initial conditions ψ_m^0 at each time layer t_n. The following sequence of actions is performed at each time-step with number n.

On the *first step*, we explicitly calculate Θ_m^{n+1} for all m from the third equation of the system (7):

$$\Theta_m^{n+1} = \left[-\frac{-2\Theta_m^n + \Theta_m^{n-1}}{h_t^2} - \bar{\gamma}\frac{-\Theta_m^n}{h_t} - \bar{\omega}^2\frac{\left|\psi_m^n\right|^2}{\bar{m}h_x}\right] \times \left[\frac{1}{h_t^2} + \frac{\bar{\gamma}}{h_t} + \bar{\omega}^2\right]^{-1}. \tag{8}$$

On the *second step*, we substitute found Θ_m^{n+1} to the second equation. The resulting system of $N = l - 1$ algebraic equations

$$\hat{A}\vec{X} = \vec{D}; \quad \hat{A} = \begin{bmatrix} b_1 & c_1 & 0 & \ldots & 0 \\ a_2 & b_2 & c_2 & \ldots & 0 \\ 0 & a_3 & b_3 & \ldots & 0 \\ \ldots & \ldots & \ldots & \ldots & \ldots \\ 0 & 0 & 0 & \ldots & b_N \end{bmatrix}; \vec{D} = \begin{bmatrix} d_1 \\ d_2 \\ d_3 \\ \ldots \\ d_N \end{bmatrix}; \vec{X} = \begin{bmatrix} \chi_1 \\ \chi_2 \\ \chi_3 \\ \ldots \\ \chi_N \end{bmatrix} \tag{9}$$

with coefficients

$$\begin{gathered} a_m = 1, \quad b_m = -2, \quad c_m = 1, \quad d_m = \Theta_m \cdot h_x^2, \quad m = 2, \ldots, N-1 \\ b_1 = 1, \quad c_1 = 0, \quad d_1 = 0, \quad a_N = -1, \quad b_N = 1, \quad d_N = 0. \end{gathered} \tag{10}$$

is solved to calculate the $\chi_m = \varphi_m^{n+1}$, $m = 1, 2, \ldots, N$.

Finally, on the *third step*, the values of φ_m^{n+1} are substituted to the first equation of system (7). The resulting algebraic system (9) with coefficients

$$\begin{gathered} a_m = \frac{i\sigma}{2\bar{m}h_x^2}, \quad c_m = \frac{i\sigma}{2\bar{m}h_x^2}, \quad b_m = \frac{1}{h_t} + \frac{i\sigma\left(2 - 2h_x\dfrac{\bar{m}r_{00}\varphi_m^{n+1}}{\tilde{\epsilon}\bar{m}}\right)}{2\bar{m}h_x^2}, \\ d_m = \frac{\psi_m^n}{h_t} + \frac{i(1-\sigma)\left(2h_x\dfrac{\bar{m}r_{00}\varphi_m^n\psi_m^n}{\tilde{\epsilon}\bar{m}} + \psi_{m+1}^n - 2\psi_m^n + \psi_{m-1}^n\right)}{2\bar{m}h_x^2}, \quad m = 2, \ldots, N-1, \\ b_1 = 1, \quad c_1 = 0, \quad d_1 = 0, \quad a_N = 0, \quad b_N = 1, \quad d_N = 0. \end{gathered} \tag{11}$$

is solved with respect to $\chi_m = \psi_m^{n+1}$, $m = 1, 2, \ldots, N$. Then the procedure is repeated for the next value of n.

To start the calculations it is necessary to set the values of φ_m^0. In the papers [5, 6] initial condition was varied in order to reproduce the theoretically predicted and experimentally measured behavior of the physical characteristics of the hydrated electron, depending on the time. In [4, 6], the calculations were also carried out, for methodological purposes, with the initial conditions in the form of stationary solutions of (5).

Parallel Algorithm

Parallel implementation of the above numerical scheme has been done in [10] on the basis of MPI technology. Numerical solution of three-diagonal algebraic equations (9) on the second and third steps of the algorithm is based on the partition method [7]. The idea of this approach is as follows. The equations of system (9) of N linear algebraic equations with a three-diagonal matrix $\hat{A}$ are distributed between parallel processors (MPI-processes). Let P is the number of parallel MPI-processes with ranges $p = 0, 1, ..., P-1$. Let $\Delta = \lfloor N/P \rfloor$.

Stage 1 (parallel). Transformation of Δ-blocks.

Each MPI-process of the range $p < (N \bmod P)$ is working, in parallel regime, with lines of matrix $\hat{A}$ with numbers i_p between $i_{min} = p \cdot (\Delta + 1) + 1$ and $i_{max} = (p + 1) \cdot (\Delta + 1)$; parallel MPI-processes of the range $p \geq (N \bmod P)$ transform lines of matrix $\hat{A}$ with numbers i_p from $i_{min} = p \cdot \Delta + (N \bmod P) + 1$ to $i_{max} = (N \bmod P) + (p + 1) \cdot \Delta$. At each group of lines associated with p-process, the block of nonzero elements has a size of $\Delta \times \Delta$ or $(\Delta + 1) \times (\Delta + 1)$.

Each Δ-fragment is transformed from the three-diagonal structure to the form with non-zero elements only in the main diagonal of the Δ-block and in vertical columns on the left and right borders of the block. For instance, in case of $\Delta = 5$ the matrix $\hat{A}$ of the form

$$\left[\begin{array}{ccccc|ccccc|c}
b_1 & c_1 & 0 & 0 & 0 & 0 & 0 & 0 & 0 & 0 & \ldots \\
a_2 & b_2 & c_2 & 0 & 0 & 0 & 0 & 0 & 0 & 0 & \ldots \\
0 & a_3 & b_3 & c_3 & 0 & 0 & 0 & 0 & 0 & 0 & \ldots \\
0 & 0 & a_4 & b_4 & c_4 & 0 & 0 & 0 & 0 & 0 & \ldots \\
0 & 0 & 0 & a_5 & b_5 & c_5 & 0 & 0 & 0 & 0 & \ldots \\
\hline
0 & 0 & 0 & 0 & a_6 & b_6 & c_6 & 0 & 0 & 0 & \ldots \\
0 & 0 & 0 & 0 & 0 & a_7 & b_7 & c_7 & 0 & 0 & \ldots \\
0 & 0 & 0 & 0 & 0 & 0 & a_8 & b_8 & c_8 & 0 & \ldots \\
0 & 0 & 0 & 0 & 0 & 0 & 0 & a_9 & b_9 & c_9 & \ldots \\
0 & 0 & 0 & 0 & 0 & 0 & 0 & 0 & a_{10} & b_{10} & \ldots \\
\hline
\ldots & \ldots & \ldots & \ldots & \ldots & \ldots & \ldots & \ldots & \ldots & \ldots & \ldots
\end{array}\right] \tag{12}$$

is transformed to the following structure:

$$\left[\begin{array}{ccccc|ccccc|c}
b'_1 & 0 & 0 & 0 & c'_1 & 0 & 0 & 0 & 0 & 0 & \ldots \\
a'_2 & b'_2 & 0 & 0 & c'_2 & 0 & 0 & 0 & 0 & 0 & \ldots \\
a'_3 & 0 & b'_3 & 0 & c'_3 & 0 & 0 & 0 & 0 & 0 & \ldots \\
a'_4 & 0 & 0 & b'_4 & c'_4 & 0 & 0 & 0 & 0 & 0 & \ldots \\
a'_5 & 0 & 0 & 0 & b'_5 & c'_5 & 0 & 0 & 0 & 0 & \ldots \\
\hline
0 & 0 & 0 & 0 & a'_6 & b'_6 & 0 & 0 & 0 & c'_6 & \ldots \\
0 & 0 & 0 & 0 & 0 & a'_7 & b'_7 & 0 & 0 & c'_7 & \ldots \\
0 & 0 & 0 & 0 & 0 & a'_8 & 0 & b'_8 & 0 & c'_8 & \ldots \\
0 & 0 & 0 & 0 & 0 & a'_9 & 0 & 0 & b'_9 & c'_9 & \ldots \\
0 & 0 & 0 & 0 & 0 & a'_{10} & 0 & 0 & 0 & b'_{10} & \ldots \\
\hline
\ldots & \ldots & \ldots & \ldots & \ldots & \ldots & \ldots & \ldots & \ldots & \ldots & \ldots
\end{array}\right] \tag{13}$$

The respective arithmetic operations are also carried out under the vector $\vec{D}$ of system (9).

Stage 2 (serial). Formation of auxiliary matrix and solution of respective algebraic system.

From the lines $i_p = i_{min}$ and $i_p = i_{max}$ of each p-group, the auxiliary small-dimension matrix of three-diagonal

structure is constructed in the 0-process. Respective system of algebraic equations has the form:

$$\begin{bmatrix} b'_1 & c'_1 & 0 & 0 & 0 & ... & 0 & 0 & 0 \\ a'_5 & b'_5 & c'_5 & 0 & 0 & ... & 0 & 0 & 0 \\ 0 & a'_6 & b'_6 & c'_6 & 0 & ... & 0 & 0 & 0 \\ 0 & 0 & a'_{10} & b'_{10} & c'_{10} & ... & 0 & 0 & 0 \\ ... & ... & ... & ... & ... & ... & ... & ... & ... \\ 0 & 0 & 0 & 0 & ... & ... & a'_{N-4} & b'_{N-4} & c'_{N-4} \\ 0 & 0 & 0 & 0 & ... & ... & 0 & b'_N & c'_N \end{bmatrix} \times \begin{bmatrix} \chi_1 \\ \chi_5 \\ \chi_6 \\ \chi_{10} \\ ... \\ \chi_{N-4} \\ \chi_N \end{bmatrix} = \begin{bmatrix} d'_1 \\ d'_5 \\ d'_6 \\ d'_{10} \\ ... \\ d'_{N-4} \\ d'_N \end{bmatrix}. \quad (14)$$

System (14) is numerically solved, in serial regime, by means of standard Thomas method with respect to elements χ_i ($i = i_{min}$ and $i = i_{max}$ of each p-group). The solutions are scattered to all MPI-processes.

Stage 3 (parallel). Calculation of solutions in Δ-blocks.

Each p-process obtains solutions χ_i ($i = i_{min}$ and $i = i_{max}$) from 0-process and calculates, recursively, all remaining elements of the vector $\vec{X}$ inside its block.

So, parallel part of the algorithm includes the transformation of elements of matrix $\hat{A}$ to the form (13) and the final calculation of the solutions inside each p-group. The serial part of the algorithm associated with the formation of an auxiliary matrix in 0-process and the solution of respective system of algebraic equation, is carried out by the process of range $p = 0$. Interaction between parallel processes is needed at the stage of construction of the auxiliary algebraic system and for the scattering of solutions of this system to all processes.

Naturally, the calculations by the formula (8) in spatial nodes m are also distributed between parallel MPI-processes.

NUMERICAL RESULTS

Efficiency of Parallel Optimization

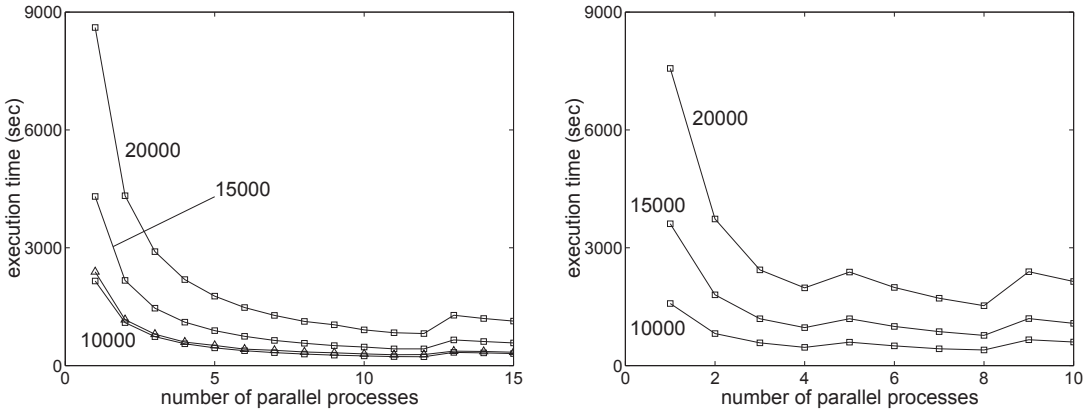

FIGURE 1. Left panel: dependence of the execution time on the number of parallel processors (MPI-processes) for the number of x-nodes $N = 10000$, 15000, 20000. □ – calculations on CICC-cluster (LIT, JINR, Dubna); △ – calculations on the CPU-blade of HybriLIT heterogenous cluster (LIT, JINR, Dubna) with $N = 10000$. Right panel: the same as in the left panel, but for the 4-core Intel(R) Core(TM) i73630QM CPU

Obviously, a number of serial arithmetic operations at the stage 2 of the above algorithm is growing proportionally P, *i.e.,* extremely high acceleration of calculations on multi-processor systems is not available. Nevertheless, in the case of relatively small number of parallel processes ($P << N$) one can expect a decreasing the execution time proportionally $1/P$.

Numerical experiments with different number of computing nodes are made on the multiprocessor cluster CICC[1]. Execution time versus the number of parallel computing nodes for different parameters for the finite-difference scheme is shown by squares in Figure 1 (left panel) to demonstrate effectiveness of the parallel C++/MPI code.

We also made calculations with $N = 10000$ on the CPU-blade of the heterogenous cluster HybriLIT[2]. Results are shown in Figure 1 (left panel) by triangles. It is seen that the execution time on both clusters is decreasing hyperbolically while $P < 13$. The calculations with $12 \leq P \leq 50$ [10] show that the further increasing of P is not effective because of a growing share of serial calculations.

The same calculations have been performed on the Intel(R) Core(TM) i73630QM CPU (4 physical cores, 8 threads) in order to estimate a perspective of utilizing of this system in further numerical simulations. P-dependence of the execution time is presented on the right panel of Figure 1. The execution time is decreased proportionally $1/P$ while $P < 5$. When P extends number of physical cores the dependence of execution time versus P is close to a constant.

So, the maximal acceleration (10 times) is achieved in the case of 12 parallel processes on multi-CPU systems CICC and HybriLIT, and the 4-time speed up is available on the 4-core one-CPU system.

Stationary Solutions and Integral of Energy

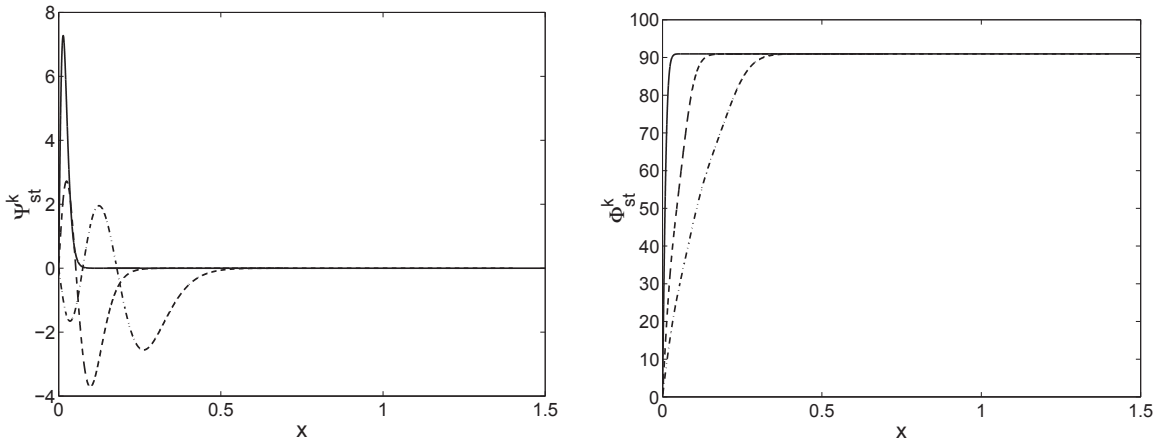

FIGURE 2. Solutions of the eigenvalue problem (16), (17) with $k = 0$ (solid line), $k = 1$ (dashed), and $k = 2$ (dash-dotted). Left panel: $\Psi^k_{st}(x)$; right panel: $\Phi^k_{st}(x)$

It can be shown that the initial conditions for system (5) in the form

$$\psi(x,t)|_{t=0} = \Psi_k(\cos(\lambda_k\xi) + i\sin(\lambda_k\xi)), \qquad \Theta(x,t)|_{t=0} = -\frac{\Psi_k^2}{x}, \qquad \frac{\partial}{\partial t}\Theta(x,t)\Big|_{t=0} = 0, \tag{15}$$

is time-independent, *i.e.,* it does not change in time. Here Ψ_k is the eigenfunction of the eigenvalue problem

$$\left[\frac{d^2}{dx^2} - 2\bar{m}\lambda + 2\bar{m}\frac{r_{00}}{\tilde{\epsilon}}\frac{\Phi_{st}(x)}{x}\right]\Psi_{st}(x) = 0, \qquad \frac{d^2}{dx^2}\Phi_{st}(x) = -\frac{\Psi^2_{st}(x)}{x}, \qquad 0 \leq x \leq \infty, \tag{16}$$

[1]Central Information Computer Complex (CICC) of Laboratory of Information Technologies of the Joint Institute for Nuclear Research (Dubna) includes more than 600 2-, 4-, 6-, and 8-Core Xeon processors, see http://lit.jinr.ru/view.php?var1=comp&var2=ccic&lang=lat&menu=ccic/menu&file=ccic/linux/archit_appar for details. Our calculations were performed on the 80-units server of 2-processor Xeon X5650 units (6 cores per processor).

[2]Heterogenous cluster HybriLIT (Laboratory of Information Technologies of the Joint Institute for Nuclear Research, Dubna) consists of four computational nodes including three nodes with graphic processors, see http://hybrilit.jinr.ru/en/ for details. Our calculations were performed on the HybriLIT CPU-blade of two 12-core Intel Xeon E5-2695v2 processors.

with the boundary conditions and the normalization condition as follows

$$\Psi_{st}(0) = 0\,,\ \Phi_{st}(0) = 0\,, \quad \Psi_{st}(\infty) = 0\,,\ \Phi'_{st}(\infty) = 0\,, \quad \int_0^\infty \Psi^2_{st}(x)dx = 1\,, \tag{17}$$

where k – the number of zeroes of eigenfunction Ψ_{st}, λ_k – the corresponding eigenvalue, ξ – an arbitrary factor, which we assumed to be $\pi/4$ in our calculations.

In order to verify the correctness of the numerical scheme, we obtained three solutions for problem (16), see Figure 2, with the number of zeroes $k = 0, 1, 2$ using the continuous analogue of the Newton method [11]. The corresponding eigenvalues are

$$\lambda_0 = 3625.55; \quad \lambda_1 = 685.97; \quad \lambda_2 = 279.01.$$

Using these solutions, we constructed the initial conditions (15) and carried out the test calculations, as a result of which we established that, when choosing the steps of the discrete mesh with respect to x and t, respectively, $h_x = 10^{-5}$ and $h_t = 10^{-7}$ the shapes of functions (15) remain unchanged in numerical simulation during a physically significant interval of time ($2 \cdot 10^7$ time steps). This confirms the correctness of the numerical approach and the corresponding MPI/C++ code.

The energy integral is calculated in accordance with the formula

$$W(t) = \frac{1}{2\bar{m}} \int \left| \frac{\partial\psi(x,t)}{\partial x} \right|^2 dx - \frac{r_{00}}{\tilde{\epsilon}} \int \frac{\varphi(x,t)\,|\psi(x,t)|^2}{x}\, dx. \tag{18}$$

Theoretical estimation of the ground state energy (case $k = 0$) is $W = -3.637$ eV [6]. Our numerical result is $W = -3.638$ eV that is in good agreement with the theoretical prediction.

Calculation of Absorption and Radius

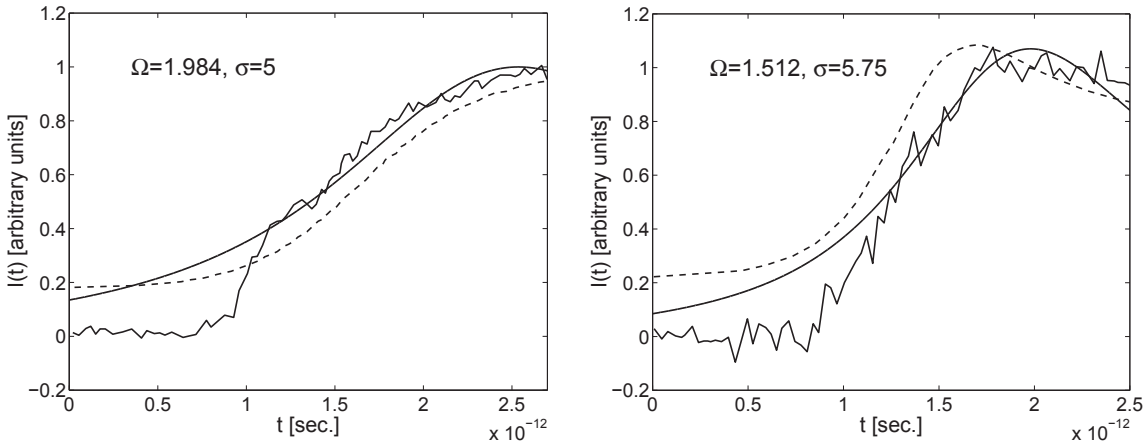

FIGURE 3. Evolution of the light absorption by a hydrated electron for $\Omega = 1.984$ eV, $\sigma = 5$ (left panel) and for for $\Omega = 1.512$ eV, $\sigma = 5.75$ (right panel). The broken curve corresponds to the experimental data [3], the solid smooth curve – to our numerical results, and the dashed curve – to the theoretical approximation [2]

To reproduce the experimental values of the intensity of light absorption by a hydrated electron, we chose the initial conditions of the wave function ψ in the Gaussian form. The initial condition for the function Θ is analogous to (15). The initial value of φ is solution of the second equation of system (5) with $\psi(x, 0)$ on the right-hand side. Accounting for the spherical symmetry and scaling factor, the function ψ at $t = 0$ is calculated as follows:

$$\psi(x, 0) = F_g(\tilde{x})\ \sqrt{4\pi}\,\tilde{x}\ \sqrt{r_{00}}, \quad \tilde{x} = x\, r_{00}, \tag{19}$$

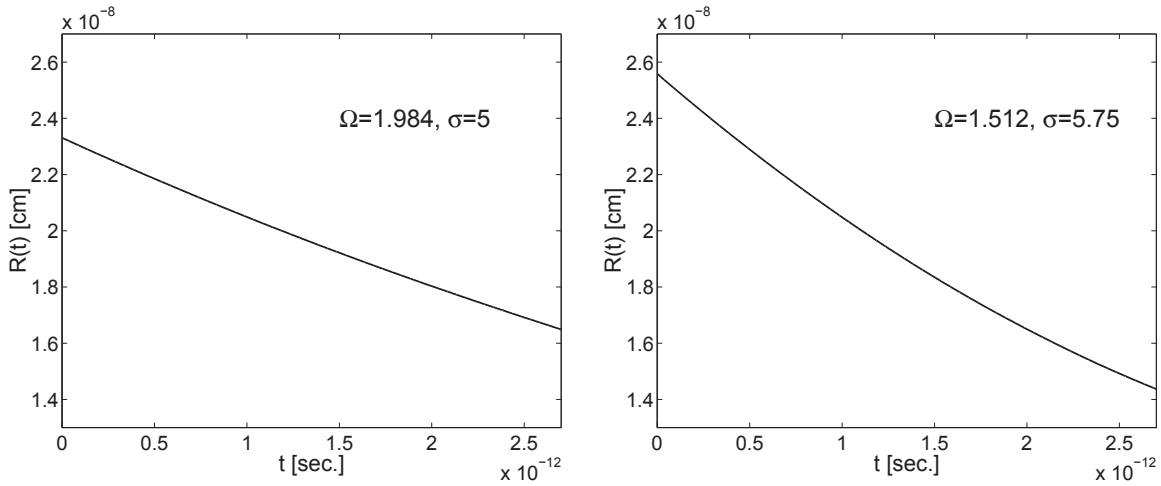

FIGURE 4. Dependence $R(t)$ for the case of $\Omega = 1.984$ eV, $\sigma = 5$ (left panel) and for $\Omega = 1.512$ eV, $\sigma = 5.75$ (right panel)

where

$$F_g(x) = \left(\frac{2}{\pi}\right)^{3/4} \frac{1}{\sigma^{3/2}} \exp(-x^2/\sigma^2). \tag{20}$$

The parameter σ was chosen to reproduce, in the computer simulation, the time dependence of the light absorption by water measured in [3].

The expression used to calculate the intensity has the form [2]:

$$I(\Omega, t) = \frac{4\Omega^2\gamma_s^2}{\left(W(t)^2 - \Omega^2\right)^2 + 4\Omega^2\gamma_s^2}, \tag{21}$$

where $\gamma_s = 0.38$ eV is the width of the absorption band of the hydrated electron and Ω has the physical sense of the light frequency of a scanning laser at which light is absorbed by the hydrated electron.

The calculations were carried out for $\Omega = 1.984$ eV and for 1.512 eV. For these two cases, Figure 3 (reproduced from [6]) shows the results of numerical simulation in comparison with the experimental data [3] and the theoretical estimations [2].

The time-dependence of the hydrated electron size (radius), is determined (in cm) via the wave function Ψ by the integral

$$R(t) = r_0 \int |\psi|^2 \, r \, dr. \tag{22}$$

The radius of hydrated electron in dependence of time is shown Figure 4 for $\Omega = 1.984$ eV, $\sigma = 5$ (left panel) and for $\Omega = 1.512$ eV, $\sigma = 5.75$ (right panel). It can be seen that the value of the radius in both cases decreases with increasing t. Initial value of $2.4 \div 2.6 \cdot 10^{-8}$ cm as well as a final one of $1.5 \div 1.7 \cdot 10^{-8}$ cm are close to the theoretical estimate of $2 \div 3 \cdot 10^{-8}$ cm. Thus, the approach described above makes it possible to adequately reproduce the hydrated electron radius and the dynamics of the light absorption by a hydrated electron.

SUMMARY

We show that the polaron model of formation of hydrated electron states on the basis of the nonlinear PDEs system, provides realistic estimations of energy, radius and light absorbtion. Results of numerical simulations of light absorption process by photoexcited hydrated electrons are in reasonable agreement with the experimental data. The model can be used for further calculations and predictions of the dynamics of polaron states in the aquatic medium and in other condensed media. MPI-based parallel algorithm provides the ten-time acceleration in comparison with the serial calculations.

ACKNOWLEDGMENTS

The work is partially supported by the Program "JINR – Bulgaria" and Russian Foundation for Basic Research (grants 13-01-00595, 13-01-00060 and 13-07-00256). The work of P.Kh.Atanasova is supported by project NI15-FMI-004.

REFERENCES

[1] A. K. Pikaev, *The Solvated Electron in Radiation Chemistry*, World University, Jerusalim, 1970.
[2] V. D. Lakhno (2007) *Chem. Phys. Lett.* **437**, 198–202.
[3] F. H. Long, H. Lu, and K. B. Eisenthal (1990) *Physical Revew Letters* **64**(12), 1469–1472.
[4] I. V. Amirkhanov, E. V. Zemlyanaya, V. D. Lakhno *et al.* (2011) *Journal of Surface Investigation: X-ray, Synchrotron and Neutron Techniques* **5**(1), 60–64.
[5] A. V. Volokhova, E. V. Zemlyanaya, V. D. Lakhno *et al.* (2014) *Komp'yut. Issled. Modelir.* **6**(2), 253–261. [in Russian]
[6] V. D. Lakhno, A. V. Volokhova, E. V. Zemlyanaya *et al.* (2015) *Journal of Surface Investigation: X-ray, Synchrotron and Neutron Techniques* **9**(1), 75–80.
[7] H. H. Wang (1981) *ACM Trans. Math. Software* **7**, 170–183.
[8] S.I. Pekar, Research in Electron Theory of Crystals, USA Department of Commerce Washington 25 D.C.: United States Atomic Energy Commision Division of Technical Information, 1963.
[9] I. S. Berezin and N. P. Zhidkov, *Computational Methods*, Vol. 2, Nauka, Moscow, 1959. [in Russian]
[10] A. V. Volokhova, E. V. Zemlyanaya, and V. S. Rikhvitskij (2015) *Computational Methods and Programming* **16**, 281–289. [in Russian]
[11] I. V. Puzynin, I. V. Amirkhanov, E. V. Zemlyanaya *et al.* (1999) *Phys. Part. Nucl.* **30**, 87.